Journal of the Australian Ceramic Society (2021) 57:1039–1047
https://doi.org/10.1007/s41779-021-00604-2

RESEARCH

Characterization of multilayer Al doping in ZnO

Ebru Şenadım Tüzemen [1,2] · Günay Merhan Muğlu [3] · B. Özgür Alaydın [1,2] · Didem Altun [4] · Selda Kılıç Çetin [5] · Emre Gür [6]

Received: 26 December 2020 / Revised: 1 March 2021 / Accepted: 12 April 2021 / Published online: 24 April 2021
© Australian Ceramic Society 2021

Abstract
ZnO, ZnO/Al, Al/ZnO/Al, and ZnO/Al/ZnO samples were deposited on c-plane sapphire and Si substrates by radio frequency magnetron sputtering (RFMS) using ZnO target. In order to form doped ZnO:Al thin films, these grown samples were annealed at temperatures of 450°C for 1 h to let diffuse Al atoms into the ZnO. After annealing homogeneous Al, diffusion is observed for the sample having Al layer at the top and the bottom of the ZnO from the cross-sectional SEM images. The effects of Al diffusion on structural, optical, electrical, and magnetic properties of ZnO layers were investigated by using x-ray diffraction (XRD), optical transmittance, sheet resistance, and magnetic field dependence of magnetization (*M(H)*) measurements. After annealing, the optical transmissions of samples were higher than 60% in the visible and near-infrared region for all samples. The sheet resistance measurement results showed that the conductivity of Al/ZnO/Al deposited on sapphire was found to be 2.64×10^{1} $(\Omega)^{-1}$ after annealing. The magnetism measurement results in that all samples show a weak ferromagnetic behavior except for the Al/ZnO/Al sample, which is attributed to the interface exchange coupling between the layers.

Keywords Aluminum diffusion · ZnO · Al doping in ZnO · Magnetron sputtering · Ferromagnetism

Introduction

One of the most studied oxide materials, ZnO, has numerous advantages in terms of material properties considered such as its high optical transmittance property in the visible region as well as being cheap and non-toxic material. In addition, ZnO has many important properties for technological applications especially for electro-optical devices such as large exciton binding energy (60 meV), high ionicity, and direct wide band gap (3.37 eV) [1–3]. Solar cells [4], field-effect transistor [5], bio-sensor [6], supercapacitor [7], and p-n junction [8] applications are among some device applications of ZnO. On the other hand, it is possible alloying ZnO with a variety of elements in order to change its bandgap energy such as Mg and Cd elements [9].

Since oxidation of Zn is very easy, there are a variety of deposition techniques actively used to grow ZnO. Some of these techniques are magnetron sputtering [10], pulsed laser deposition [11], sol-gel solution deposition [12], atomic layer deposition [13], successive ionic layer adsorption reaction (SILAR) method [14], and pulsed filtered cathodic vacuum arc deposition [15]. Magnetron sputtering is one of the most commonly used methods, because the alloys having different evaporation velocity at different vapor pressures can be successfully deposited without changing their composition. Furthermore, the possibility of entering macroparticles into the film structure is very low in this method. The quality and structure of the film obtained by the sputtering are excellent and the adhesion to the substrate is quite good [1].

One of the most promising potentials for the ZnO material systems is usability as an alternative transparent conductive oxide instead of indium tin oxide due to the limited availability of In element. In this case, enhancing the electrical conductivity of ZnO is important without changing the transparency of the material. For this aim, ZnO is commonly doped

✉ Ebru Şenadım Tüzemen
esenadim@cumhuriyet.edu.tr

[1] Department of Physics, Faculty of Science, Sivas Cumhuriyet University, 58140 Sivas, Turkey

[2] Nanophotonic Application and Research Center, Sivas Cumhuriyet University, 58140 Sivas, Turkey

[3] Department of Medical Techniques and Services, Hınıs Vocational College, Ataturk University, 25250 Erzurum, Turkey

[4] Sivas Vocational College, Sivas Cumhuriyet University, 58140 Sivas, Turkey

[5] Central Research Laboratory, Çukurova University, 01330 Adana, Turkey

[6] Department of Physics, Faculty of Science, Ataturk University, 25240 Erzurum, Turkey

with aluminum or gallium [11, 12, 16]. There are more interests on Al-doped ZnO (AZO) thin films, since it has achieved better conductivity values compared to that of Ga doping [11, 12]. However, it is important to notice that the efficient and uniform doping is required for the reliability of the materials. Many approaches have been employed for doping of ZnO with Al such as adding the Al source into the solution for solution-based synthesized materials [17], using a ZnO:Al sputtering targets at different Al concentrations [11], and using two separate sources in growth such as atomic layer deposition, pulsed laser deposition, and sputtering. One promising strategy for better doping schemes is to employ a multilayer growth to enhance the diffusion throughout the thickness of the material. The multilayer growth strategy has very good potential in terms of producing a film with high conductance and transmittance as shown by the ZnO:Al/Ag/ZnO:Al [18]. ZnO/ZnO:Al/ZnO nanostructure-based film was also prepared by electroless process and, however, no electrical conductivity data was presented [19]. ZnO/Al/ZnO was grown by thermal evaporation to produce high-conductivity transparent material. Transmittance at the visible region of 75% and the resistivity of 2.9×10^{-3} Ω cm was achieved [20]. The effect of the middle layer Al thickness between 1 and 10 nm in ZnO/Al/ZnO multilayer structure was also shown [21]. The 10-nm thickness is shown be a highly improved performance compared to other samples.

Although, it is showing promising advantages of multilayer growth for doping in order to obtain high conductance and transmittance materials, there are scarce reports showing the effects of the multilayer growth effects. In the present study, different strategies were applied in order to investigate the effects of Al multilayer on the electrical and optical properties as well as magnetic properties. Al metals from the top, bottom, and middle of the ZnO thin films grown by magnetron sputtering with the same thicknesses were prepared, namely, ZnO/substrate, ZnO/Al/ZnO/substrate, ZnO/Al/substrate, and Al/ZnO/Al/substrate samples.

Experimental details

Thin films are deposited by radio frequency magnetron sputtering (RFMS) technique on the c-plane sapphire (c-Al_2O_3) and (100) Si substrates. The distance between the substrate and the target was 6 cm and kept constant for all the growths. The substrate was heated to 300 °C. The base pressure was ~5×10^{-7} Torr achieved by a liquid nitrogen finger. RF power for the growth was 60 W and the growth pressure was 20.0 mTorr. Sputtering was started after the inert gas entrance to the chamber. ZnO (200nm) (Z), ZnO (200nm)/Al (10nm) (ZA), ZnO (200nm)/Al (10nm)/ZnO (200nm) (ZAZ), and Al(10nm)/ZnO(200nm)/Al(10nm) (AZA) layers were deposited on silicon and sapphire substrates as shown in Fig. 1. Inside the parenthesis of the grown multilayer structures shows the name of the samples. Samples grown on Si substrates are named Z-Si, ZA-Si, ZAZ-Si, and AZA-Si, while the samples grown on sapphire are named Z-Sa, ZA-Sa, ZAZ-Sa, and AZA-Sa, respectively. In situ thickness measurements were done during sputtering. All the thin films were annealed at 450 °C for 1 h in air ambient condition except for bare ZnO (200nm). In order to put the differences between annealed and as-grown samples, "450" is added at the end of the sample name.

After growth, XRD studies of as-deposited and annealed samples were carried out using the Rigaku Miniflex-XRD system. Absorptions and transmissions were measured with Varian Cary 5000 model UV–VIS–NIR spectrophotometer. The measurements were done in the range of 200–800 nm and reflectance measurements were measured with DRA2500 up to 800 nm. Electrical properties of the films were performed by the HMS-3000 system using the four-point probe Van der Pauw technique. In order to determine the magnetic behavior of the samples, magnetization measurements were performed by using the vibrating sample magnetometer (VSM) option of PPMS (Quantum Design Dynacool-9T) system.

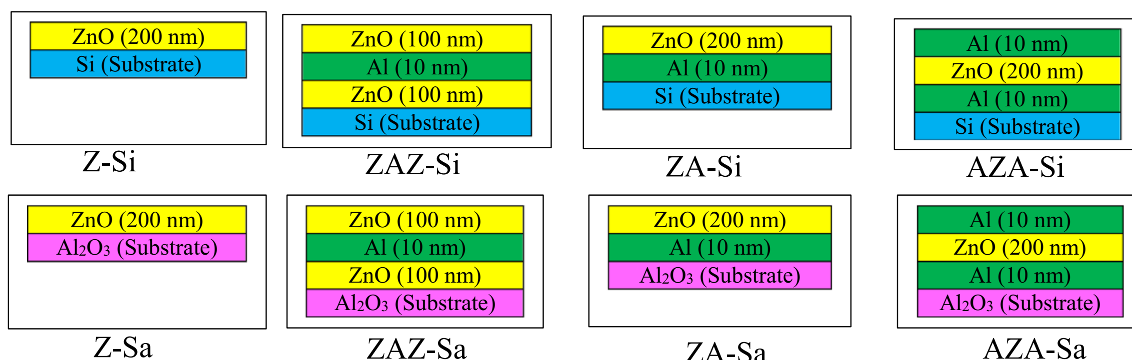

Fig. 1 Schematic representation of the samples deposited on Si and sapphire by RFMS

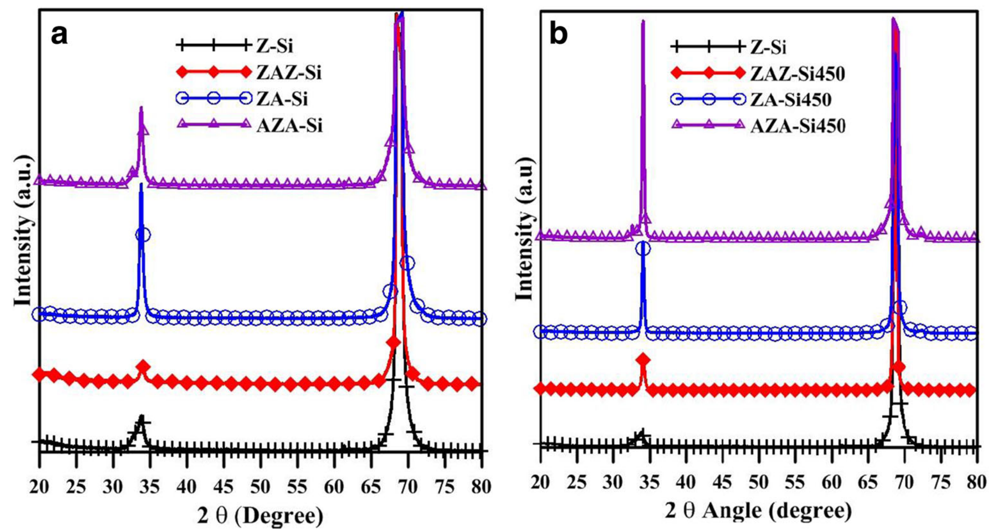

Fig. 2 XRD graphics of the multilayer samples produced on Si. **a** As-deposited. **b** Annealed

Results and discussion

Structural properties

X-ray diffraction results are represented in Fig. 2. Main peaks, which correspond to ZnO (002) plane, become sharper in samples ZAZ-Si, ZA-Si, and AZA-Si compared to that of control sample Z-Si. The incorporation of aluminum atoms into ZnO crystal as a dopant atom is most likely responsible for the change observed in XRD data. This might be due to the growth at 300 °C; Al atoms start to diffuse into the ZnO and the structural quality changes as shown in Fig. 2 a. After annealing, even sharper (002) reflection for samples ZAZ-Si, ZA-Si, and AZA-Si can be seen compared to that of sample Z-Si, as shown in Fig.2 b. At this point, there is an observed small shift in the 2θ angle compared to that of the control Z-Si thin film except for the thin film ZAZ-Si450 (Table 2). The shift means the change in the crystal structure by changing the lattice parameters. However, no change observed in the ZAZ-Si450 might be showing Al incorporation is not changing the lattice parameters in this film.

Further analysis is made by grain size evaluation. The grain size of the crystals in the films is calculated from the X-ray diffraction data by using the well-known Scherrer formula [22];

$$D = \frac{K\,\lambda}{\beta\, cos\theta}$$

where K is a constant, λ is the wavelength of the X-ray used, θ is the Bragg reflection angle, and β is the half-maximum width (FWHM) of the reflections in radians. For calculations, the K constant is taken as 0.9. The widths of the X-ray diffraction data reflect the grain size as shown in Table 1. In addition, the structural properties of samples produced on sapphire showed similar behavior with those produced on silicon. Grain size values increase after annealing except for the ZA-Si thin film.

Cross-sectional SEM analysis

In Fig. 3, the white region as indicated by cross-sectional back-scattered SEM images shows the ZnO coating on Si substrate. The approximate thickness was measured for all the ZnO samples to be ~200 nm. The interface between ZnO and Si seems to be clear and coated coherently. The upper row indicates (Fig. 3 a, b, c) the as-deposited ZnO-Al layers while the lower row (Fig. 3 d, e, f) shows the images after annealing. It is clearly seen that the ZAZ-Si and AZA-Si layers seem to

Table 1 X-ray diffraction data results of samples produced on Si

	Angle(2θ) (deg.)	d (nm)	Assignment	FWHM (deg.)	Grain size (D) (nm)
Z-Si	34.0	0.264	(002)	1.34	5.92
ZAZ-Si	33.8	0.265	(002)	0.72	11.0
ZA-Si	33.8	0.265	(002)	0.48	16.5
AZA-Si	33.8	0.265	(002)	0.49	16.2
ZAZ-Si450	34.0	0.264	(002)	0.70	11.3
ZA-Si450	33.7	0.266	(002)	0.55	14.4
AZA-Si450	33.8	0.265	(002)	0.46	17.3

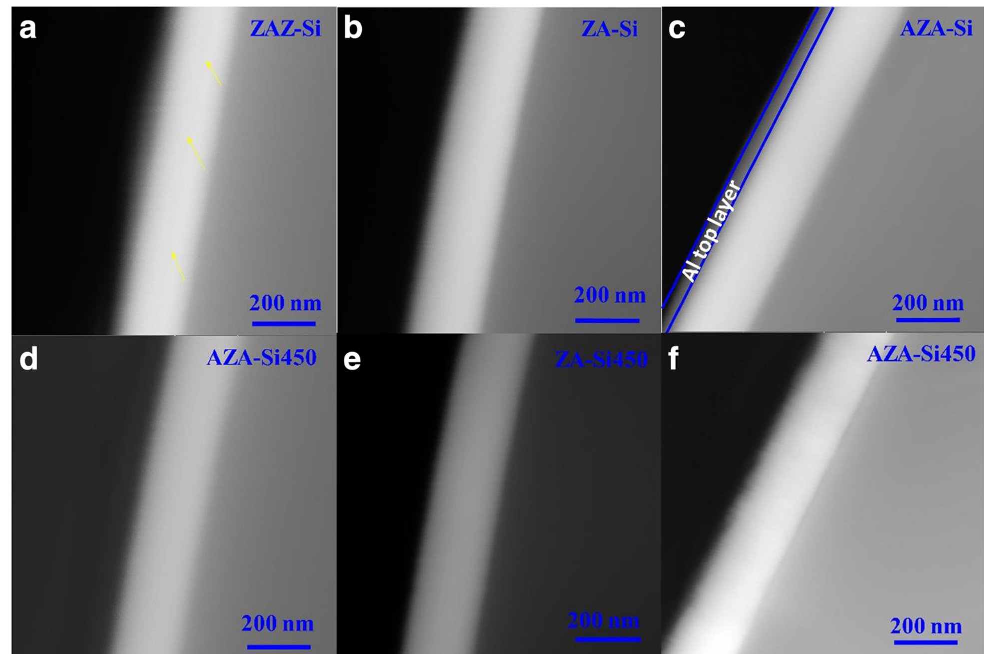

Fig. 3 The cross-sectional SEM images of **a** ZAZ-Si, **b** ZA-Si, **c** AZA-Si, **d** ZAZ-Si450, **e** ZA-Si450, and **f** AZA-Si450

have Al and ZnO layers, separately. Even a thin layer of Al about 10 nm is visible for ZAZ-Si as well as Al on the top layer in AZA-Si samples. However, the Al layer at the Si interface in AZA-Si and the ZA-Si samples is not clear. This might be due to the Al diffusion into the Si substrate during the growth, since the growth was performed at 300 °C. After annealing, no visible separate layers can be seen due to the high diffusion of the Al element into the ZnO matrix to the possible production of Al-doped ZnO layers.

The line EDS analysis taken from cross-sectional SEM images shows the distribution of elements along the line from the top of the ZnO to the inside of the substrate Si as shown in Fig. 4. The length of the line profile analysis is 800 nm. Two cross-sectional SEM images (Fig. 4 a and b) with line elemental profiling belong to as-deposited ZAZ-Si and AZA-Si samples can be seen as a representative in the figure. In both of these cross-sectional SEM images, it is seen that the intensity of the Si element increases through the Si substrate, but it is interesting to see that there is a Si element in the ZnO films which is higher at the interface and decreasing through the surface of the ZnO. This might be due to the Si diffusion into the film due to a growth temperature of 300 °C. Furthermore, it is noticed that Al element peaks in the ZAZ-Si sample in the middle of the sample, while it is on the top surface of the AZA-Si film as illustrated in the cross-sectional SEM images in the figures. When these two as-deposited samples are compared, it is seen that the Al element signal is higher in the AZA-Si sample than the ZAZ-Si throughout the ZnO thin film. Al element diffusion into the Si substrate is also seen especially in the ZnO thin film having Al layer top and bottom side (AZA-Si). This diffusion is the reason not to observe the Al layer as a separate layer at the interface between Si and ZnO.

The inset in Fig. 4b shows the line element profile after annealing the AZA-Si sample. It is seen that the Al is homogenously distributed throughout the ZnO thin film after annealing. On the other hand, Al distribution is not homogenous after annealing for those ZA-Si and ZAZ-Si films as seen in Fig. 4 c, d, and e. Line elemental profile before and after annealing for ZA-Si thin film can be seen in Fig. 4d and e. As seen in those figures, it is almost the same profile appearing before and after annealing. This is mainly due to the Al layer at the interface in ZA-Si thin film which diffuses into the Si substrate during the growth. This affects the Al distribution through the ZnO thin film and non-uniform distribution is seen. For the ZAZ-Si450 film, EDS spectra can be seen in Fig. 4 c at six different points. The first 3 spectra from the top are within the ZnO layer with a red one from the top, yellow from the middle, and the green one at the interface, while the last three bottom rows show the spectra taken from inside of the Si substrate. As seen from the figure, the Si peak increases in the most deeper spectra taken from the Si substrate (black spectrum) and all the other peaks diminish compared to that of the Si peak. Also, the Al peak intensity varies from the top to the inside Si substrate. Table 2 shows the element compositions obtained from each spectrum given in Fig. 4 c. As seen in the table, the Al content is lowest at the top of the surface and the very last row deepest in the Si substrate.

Optical properties

In optical properties of samples grown on sapphire substrate Z-Sa, ZAZ-Sa, ZA-Sa, and AZA-Sa, samples were investigated before and after annealing by measuring the absorptions and transmissions of the samples. The transparency of the

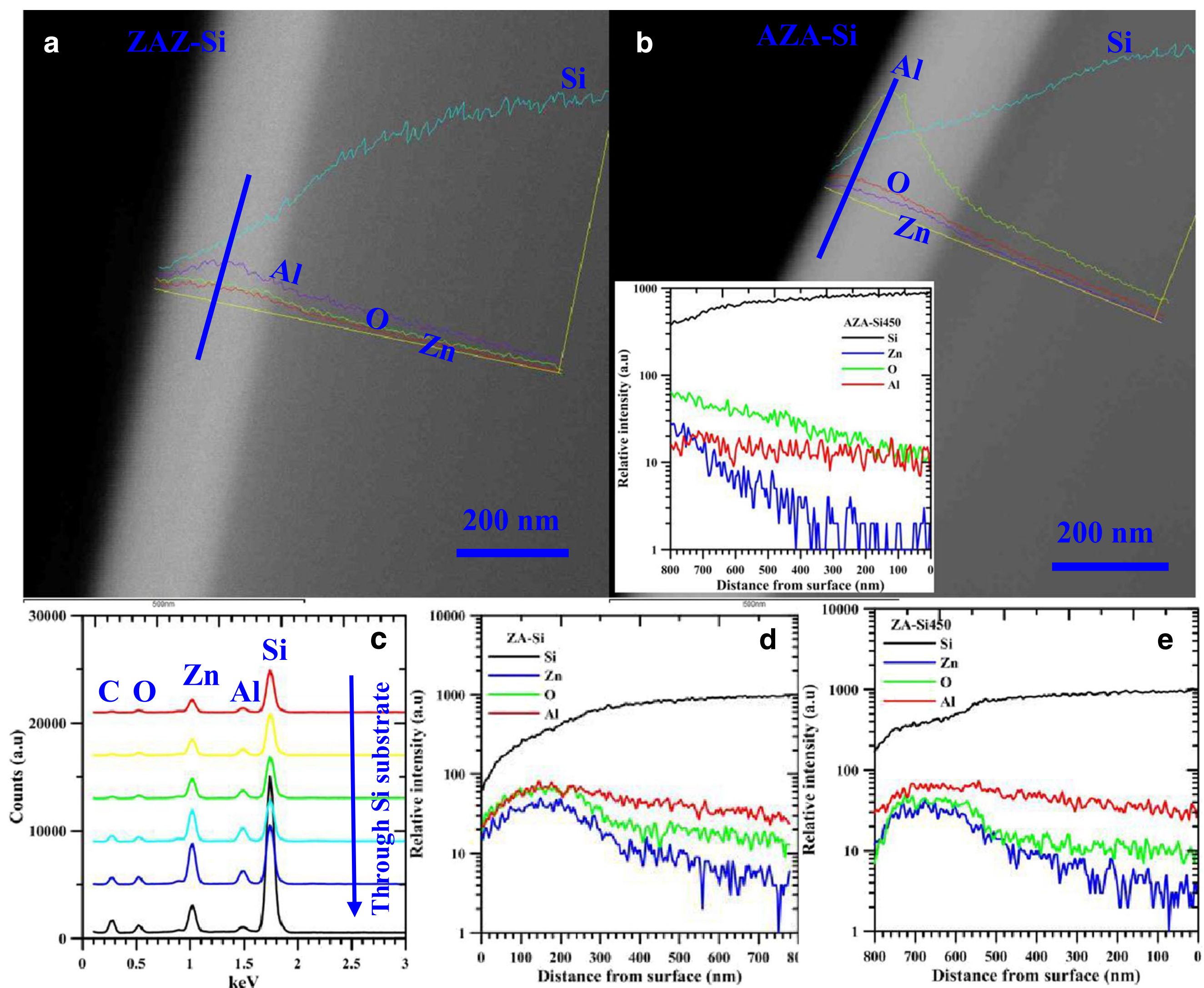

Fig. 4 Cross-sectional SEM image with line element profile. **a** ZAZ-Si. **b** AZA-Si sample, inset is element profile after annealing the sample. **c** EDS spectra of ZAZ-Si450 from six different places in cross-sectional SEM images. **d** plot for element profile for ZA-Si before annealing. **e** Plot for element profile for ZA-Si after annealing

control sample Z-Sa is around 80% in the 400–800-nm range as shown in Fig. 5. Transmission of all other as-grown multi-layer structures is lower than that of Z-Sa before annealing. After annealing, the transparency of the samples changes due to diffusion of the Al. For example, the transmission of sample ZAZ-Sa is very low for the as-grown layer after deposition due to metallic mirror behavior of Al layer, after annealing reflectance is almost identical with sample Z-Sa, which is a proof of single ZnO film phase on the substrate. For sample ZAZ-Sa, all Al atoms seem diffused in ZnO as a dopant because of observed identical transmission with bare ZnO. On the other hand, the trend of sample ZA-Sa shows that diffusion

Table 2 Compositional analysis of ZAZ-Si450 annealed sample

C (at. %)	O (at. %)	Al (at. %)	Si (at. %)	Zn (at. %)
32.86	14.28	3.83	40.78	8.25
35.78	15.12	4.66	35.50	8.94
37.68	15.09	5.79	31.79	9.65
54.31	13.01	5.53	18.16	8.99
50.23	16.51	4.34	19.84	9.08
59.28	10.97	0.68	25.60	3.47

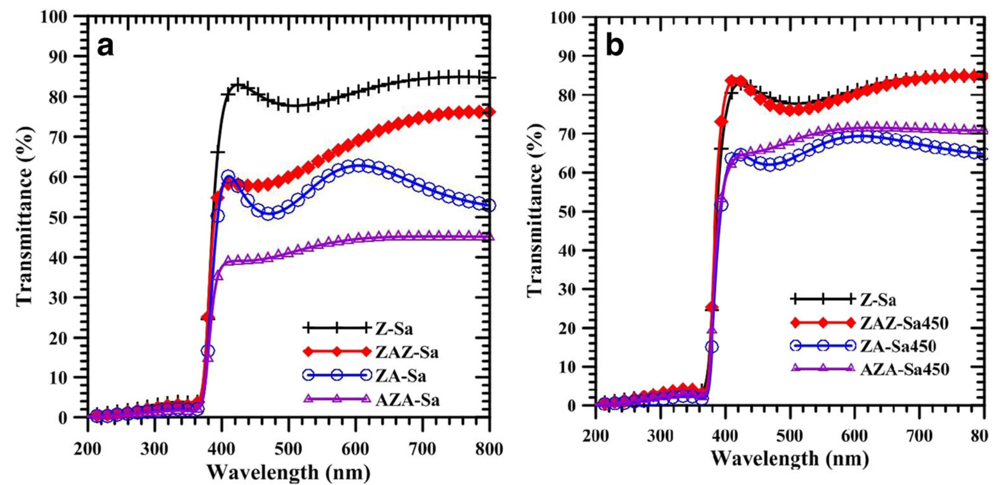

Fig. 5 Change of transmittance of films produced on sapphire according to wavelength. **a** As-deposited. **b** Annealed

is unlikely to happen during the annealing, since no significant change before and after annealing is observed in the transmission spectra as shown in Fig. 5. It seems still metallic mirror behavior of Al films observable. From these observations, it might be concluded that the bottom Al metallic structure might not be the best for Al diffusion. As it is also shown from the cross-sectional SEM images, the Al layer at the interface diffuses through the substrate during the growth. Low transmission value is observed for sample AZA-Sa probably due to the top and bottom metallic aluminum film. This change in the transmittance might be indicative of heavy Al doping. Even though the crystalline quality is improved just a bit after annealing, however, the transmission is improved significantly in sample AZA-Sa450. On the other hand, the distribution of Al is quite good and perhaps the Al quantity is very low by growing 10-nm Al in the middle instead of top and bottom as the transmittance values are compared.

In order to obtain band gap values for the samples, absorption coefficient data analysis was performed. The absorption coefficient is given as $\alpha = (1/d)$ In $(1/T)$. d is film thickness and T is transmission [20]. The absorption coefficient (α) and band gap (E_g) is proportional as given below;

$$\alpha = A\left(h\nu - E_g\right)^n / h\nu$$

Here, it is known that A is constant, $h\nu$ is photon energy, and n is 0.5 for direct band gap materials [20]. The band gap of the films was calculated by using the formula above. From Fig. 6, the value of the energy band gap is about 3.25, 3.26, 3.26, and 3.26 eV for Z-Sa, ZAZ-Sa, ZA-Sa, and AZA-Sa samples, respectively, as given in Table 3. Energy band gaps of ZnO thin films are increased with Al doped. The increase in these values may be due to the increased carrier concentration causing the Burstein-Moss effect by preventing to be full of low energy states in the conduction band [23]. It was observed that the change in the energy band gap was the most before and after annealing of the AZA-Sa and ZAZ-Sa samples.

In addition to the Tauc plots [24] used above, the first derivative plot of the transmittance [25, 26] was used to find the band gap energy values of the thin films. The change of $dT/d\lambda$ according to wavelength can be seen in Fig. 7. It is observed that the peak of the Z-Sa sample has the highest wavelength (lowest energy band gap); thus, it is decided that the change in band gap energy values occurs with the introduction to ZnO of Al. The energy band gap values are shown in Table 3. Figure 7 shows quite clearly the strong reduction in amplitude of the AZA-Sa sample.

In Fig. 8, reflectance measurements of Z-Si, ZAZ-Si, ZA-Si, and AZA-Si are shown. It is seen that the total reflection changes very much after annealing for samples ZAZ-Si. It is observed that the annealing procedure does not change the reflectance of the control sample ZnO as shown in Fig. 8. However, annealing has a significant effect on the reflectance of the sample ZA-Si450 and AZA-Si450. Samples ZA-Si450 and AZA-Si450 have the highest reflectance close to absorption edge than decreasing sharply.

Table 3 Energy band gap obtained for two different samples for all the samples

	Z-Sa	ZAZ-Sa	ZA-Sa	AZA-Sa	ZAZ-Sa450	ZA-Sa450	AZA-Sa450
E_g (eV) $(\alpha h\nu)^2$	~3.25	~3.26	~3.26	~3.26	~3.27	~3.26	~3.27
E_g (eV) $(dT/d\lambda)$	~3.25	~3.26	~3.25	~3.26	~3.27	~3.26	~3.27

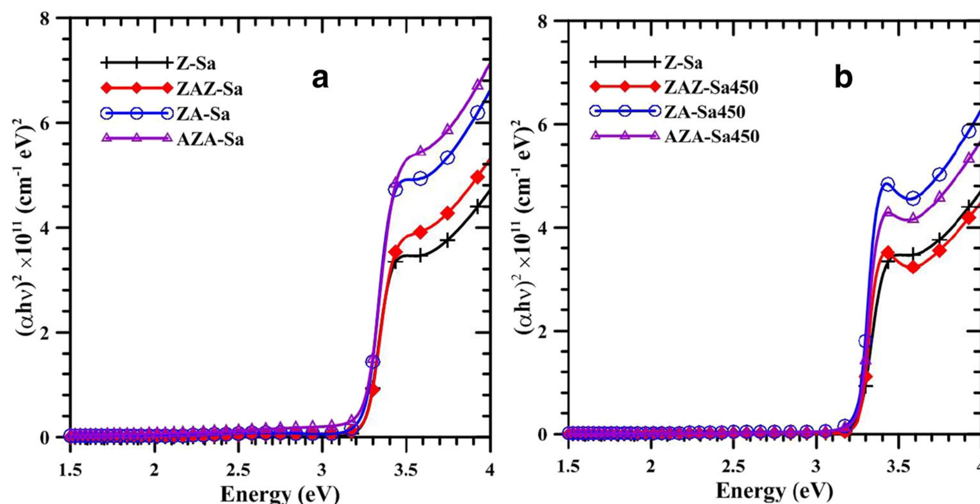

Fig. 6 A plot of $(\alpha h\nu)^2$ vs energy for **a** as-deposited and **b** annealed

Electrical properties

Hall effect measurements were conducted to characterize the electrical properties of the Z-Sa, ZAZ-Sa450, ZA-Sa450, and AZA-Sa450 samples. Measurements were made at room temperature and carried out in a constant magnetic field of 0.54 T. Hall parameters such as bulk concentration, mobility, resistivity, sheet concentration, average Hall coefficient, carrier type, and conductivity for the films were obtained and tabulated in Table 4. To ensure the reliability of the results, the Hall measurements were repeated several times for each sample.

Hall effect measurements were not applied Al top deposited as-grown thin films. Those thin films are measured after annealing, since no metallic Al layer is observed on top. Hall measurement has shown that all layers are n-doped as expected. The control sample Z-Sa, which does not have an Al-containing layer, shows background doping of around 1.3×10^{17} cm^{-3}. The highest doping is achieved for the sample AZA-Sa450 which is on the order of ~10^{19} cm^{-3} compared to that of other samples. The result might be due to the larger diffusion of Al atom into ZnO layers from the top and the bottom layer. In the present case, the mobility is highest for the sample AZA-Sa450 with the highest concentration. This might be related to the change in crystalline quality of the samples after annealing. The best Al diffusion from the transmission curves given in Fig. 5 was seen for the AZA-Sa450 sample as discussed above. It is also obtained that the lowest resistivity and highest bulk concentration is found in the AZA-Sa450 sample from electrical measurements. As a result, it can be concluded that the sample of AZA-Sa450 is the best structure to dope ZnO by Al. Although ~10^{19} cm^{-3} doping is achieved in the AZA-Sa450 thin film, the achieved resistivity value is a bit lower than the reported values in multilayer samples [18, 20, 27]. On the other hand, obtained transmittance and the mobility, 18.2 cm^2/(V.s), values are better compared to the given literatures above.

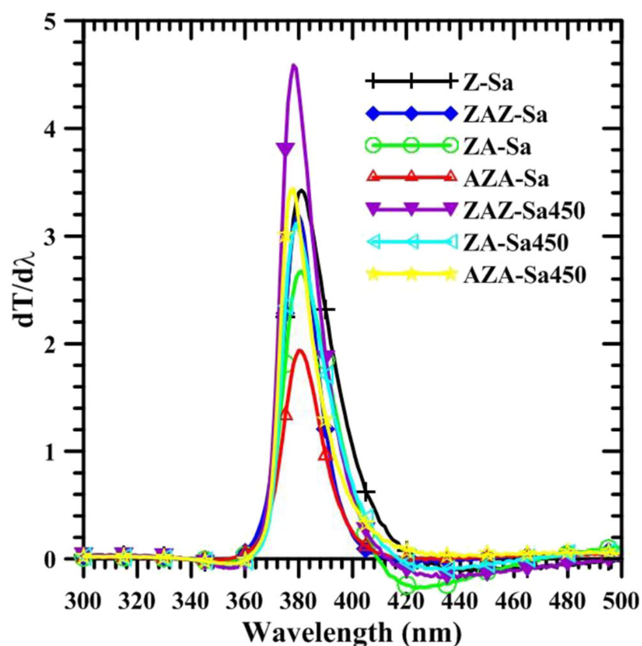

Fig. 7 Plots of the derivative of the transmittance with respect to the wavelength of the as-deposited and annealed samples

The magnetic field dependence of magnetization (*M(H)*) measurements for AZA-Sa450, ZAZ-Sa450, Z-Sa, and ZA-Sa450 samples were performed under ±5 T magnetic field at room temperature and the hysteresis curves of the samples are shown in Fig. 9. The data collected from samples was taken along the plane of the film and the hysteresis curves of the samples show weak ferromagnetic behavior. The origin of ferromagnetic behavior may be resulting from oxygen vacancies and other intrinsic defects in samples [28–31]. The saturation magnetization (M_s) of AZA-Sa450, ZAZ-Sa450, Z-Sa, and ZA-Sa450 samples is determined as 1.13×10^{-2}, 0.60×10^{-2}, 0.34×10^{-2}, and 0.25×10^{-2} emu/cm^3, respectively. The AZA-Sa450 film shows higher saturation magnetization compared to that of other samples. The strong ferromagnetism of AZA-

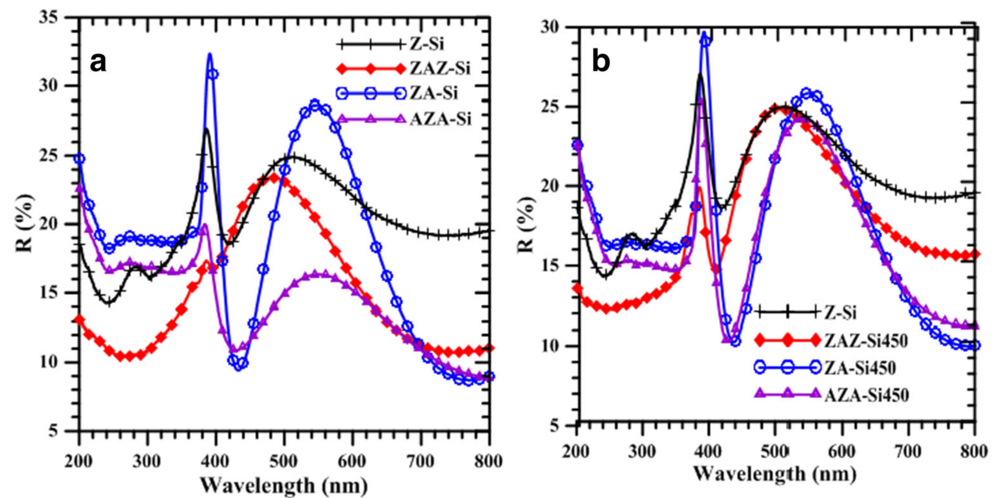

Fig. 8 Change of films produced on Si of reflectance according to wavelength. **a** As-deposited. **b** Annealed

Sa450 film compared to other samples can be attributed to the interface exchange coupling between AZA-Sa450 layers. The coercive field values (H_c) of AZA-Sa450, ZAZ-Sa450, Z-Sa, and ZA-Sa450 samples were determined to be approximately 124.22, 430.29, 627.18, and 942.12 Oe, respectively, indicating that they act as a soft ferromagnetic material. The systematic increase in H_c is likely to originate from domain wall pinning effects [32]. The remanent magnetization (M_r) of AZA-Sa450, ZAZ-Sa450, Z-Sa, and ZA-Sa450 samples was determined as 6.80×10^{-4}, 6.23×10^{-4}, 3.51×10^{-4}, and 3.38×10^{-4} emu/cm^3, respectively. It can be thought that the systematic decrease of M_r value can be considered due to the gradual decrease of saturation magnetization of the samples [33].

The effective magnetic moment (μ_{eff}) has been determined from the following equation,

$$\mu_{\text{eff}} = \frac{M_w M_s}{N_A \beta}$$

where M_w is the molecular weight, M_s is the saturation magnetization, N_A is the Avogadro's number, and β is the conversion factor (9.27×10^{-21} erg/Oe). The effective magnetic moment of AZA-Sa450, ZAZ-Sa450, Z-Sa, and ZA-Sa450 samples is calculated as 2.19×10^{-4}, 1.16×10^{-4}, 0.49×10^{-4}, and 0.48×10^{-4} μ_B, respectively. The small μ_{eff} values indicate that a very small fraction of ions are ferromagnetically coupled at the interfaces of the AZA-Sa450, ZAZ-Sa450, Z-Sa, and ZA-Sa450 films [34].

Conclusion

Different multilayer samples were grown to investigate the effective doping of ZnO with Al by the magnetron sputtering method. For this aim, ZnO(200nm) (Z), ZnO(200nm)/Al(10nm) (ZA), ZnO(100nm)/Al(10nm)/ZnO(100nm) (ZAZ), and Al(10nm)/ZnO(200nm)/Al(10nm) (AZA) samples were prepared and annealed at 450 °C for diffusion of Al into the ZnO. The diffusion of the Al at the interface through the Si substrate is observed from the cross-sectional SEM images. It is also shown that the Al distribution is quite homogeneous after annealing for the AZA-Si450 sample. This homogeneous distribution might have an effect on the enhanced crystal quality of annealed ZnO multilayer samples. It was observed that the transmittance of the grown samples varies significantly before and after annealing. The transmittance of the sample ZAZ-Sa becomes almost identical with the control sample after annealing which confirms the diffusion of the Al into the ZnO film. Hall effect measurements showed that ~10^{19} cm^{-3} concentration and 10^{-2} Ωcm resistivity were achieved in the AZA sample. The magnetic results reveal that all samples, except for the AZA sample, show a weak

Table 4 Results of the Hall effect measurements

	Z-Sa	ZAZ-Sa450	ZA-Sa450	AZA-Sa450
Bulk concentration (cm^{-3})	-1.3×10^{17}	-1.5×10^{18}	-4.7×10^{17}	-2.0×10^{19}
Mobility (cm^2/V.s)	4.0	6.8	1.8	18.2
Resistivity (Ω.cm)	12.2	6.2×10^{-1}	7.3	3.8×10^{-2}
Sheet concentration (cm^{-2})	-1.3×10^{12}	-1.5×10^{13}	-4.7×10^{12}	-9.1×10^{13}
Conductivity (1/Ω)	8.2×10^{-2}	1.6	1.4×10^{-1}	2.6×10^{1}
Average Hall coefficient (m^2/C)	-4.8×10^{1}	−4.2	-1.3×10^{1}	4.8×10^{2}
Carrier type	*n*	*n*	*n*	*n*

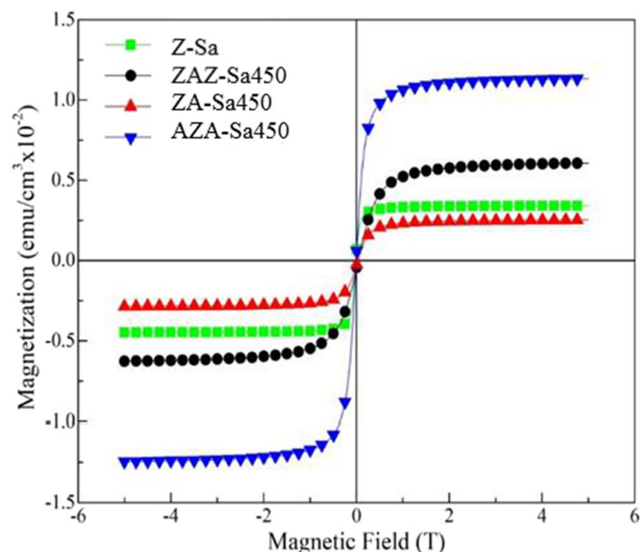

Fig. 9 The hysteresis curves of ZnO(200 nm), ZnO(100 nm)/Al(10 nm)/ZnO(100 nm), Al(10 nm)/ZnO (200 nm), and Al(10 nm)/ZnO(200 nm)/Al(10 nm), which is labeled as Z-Sa, ZAZ-Sa450, ZA-Sa450, and AZA-Sa450, respectively

ferromagnetic behavior. AZA is the sample with the strongest ferromagnetism, which is attributed to the interface exchange coupling between the layers. It is concluded that by optimizing the annealing conditions, it is possible to obtain films which have better crystal quality, conductivity, and magnetic properties. Effective and homogenous diffusion of the Al throughout the ZnO thin film showed enhanced electrical and magnetic properties in the multilayer ZnO-Al samples.

Acknowledgements This study was conducted in Ataturk University, Department of Physics, Faculty of Science, Sivas Cumhuriyet University R&D Center (CUTAM) in SEM Lab., Sivas Cumhuriyet University Nanophotonic Application and Research Center in Optic Lab and Cukurova University.

Funding This research was supported by the Scientific Research Project Fund of Sivas Cumhuriyet University under the project number F-537.

Declarations

Conflict of interest The authors declare no competing interests.

References

1. Tüzemen, S., Gür, E., Yıldırım, T., Xiong, G., Williams, R.T.: J. Appl. Phys. **100**, 103513 (2006)
2. Dong, H., Zhou, B., Li, J., Zhan, J., Zhang, L.: J. Mater. **3**, 255 (2017)
3. Demirci, S., Dikici, T., Tünçay, M.M., Kaya, N.: Appl. Surf. Sci. **507**, 145083 (2020)
4. Fathima, M.I., Wilson, K.S.J.: Vacuum. **165**, 58 (2019)
5. Yoon, J., Huang, F., Shin, K.H., Sohn, J.I., Hong, W.K.: Materials. **13**, 268 (2020)
6. Bhat, S.S., Qurashi, A., Khanday, F.A.: Trends Anal. Chem. **86**, 1 (2017)
7. Chen, X., Wang, X., Liu, F., Song, X., Cui, H.: Vacuum. **178**, 109453 (2020)
8. Tekmen, S., Gür, E., Asıl, H., Çınar, K., Coşkun, C., Tüzemen, S.: Phys. Stat. Sol. A. **207**, 1464 (2010)
9. Gür, E., Tabares, G., Arehart, A., Chauveau, J.M., Hierro, A., Ringel, S.A.: J. Appl. Phys. **112**, 123709 (2012)
10. Makino, H., Shimizu, H.: Appl. Surf. Sci. **439**, 839 (2018)
11. Kek, R., Nee, C.H., Yap, S.L., Tou, T.Y., Arof, A.K.B.H.M., Koh, S.F., Yap, S.S.: Mater. Res. Express. **5**, 116201 (2018)
12. Kraya, R., Baskar, J., Arceo, A., Katz, H.E., Thakor, N.: Thin Solid Films. **664**, 41 (2018)
13. Yıldız, D.E.: J. Mater. Sci. Mater. **29**, 17802 (2018)
14. Higgins, M., Pintor-Monroy, M.I., Quevedo-Lopez, M.: Cryst. Res. Technol. **53**, 1800039 (2018)
15. Senadim, E., Kavak, H., Esen, R.: J. Physics-Condens Matter. **18**, 6391 (2006)
16. Bruncko, J., Sutta, P., Netrvalová, M., Michalka, M., Vincze, A.: Vacuum. **159**, 134 (2019)
17. Selim, M.S., Sekhar, M.C., Raju, A.R.: Appl. Phys. A Mater. Sci. Process. **78**, 1215 (2004)
18. Kim, J.H., Moon, Y.J., Kim, S.K., Yoo, Y.Z., Seong, T.Y.: Ceram. Int. **41**, 14805 (2015)
19. Rahman, A., Jayaganthan, R., Sharma, J.V.N.: Surf. Eng. **30**, 709 (2014)
20. Al-Kuhaili, M.F., Al-Maghrabi, M.A., Durrani, S.M.A., Bakhtiari, I.A.: J. Phys. D. Appl. Phys. **41**, 215302 (2008)
21. Rwenyagila, E.R., Tuffour, B.A., Kana, M.G.Z., Ojo, O.A., Soboyejo, W.O.: J. Mater. Res. **29**, 24 (2014)
22. Gadallah, A.S., El-Nahass, M.M.: Adv. Condens. Matter Phys. **2013**, 234546 (2013)
23. Burstein, E.: Phys. Rev.. 93, 632 (1954); Moss, T. S.: Proc. Phys. Soc. London. B76, 775 (1954).
24. Kumbhar, D., Kumbhar, S., Salunke, G., Nalawade, R., Nalawade, A.: Macromol. Symp. **387**, 1800192 (2019)
25. Meriche, F., Touam, T., Chelouche, A., Dehimi, M., Solard, J., Fischer, A., Boudrioua, A., Peng, L.H.: Electron. Mater. Lett. **11**, 862 (2015)
26. Saha, B., Sarkar, K., Bera, A., Deb, K., Thap, R.: Appl. Surf. Sci. **418**, 328 (2017)
27. Seo, I., Ryu, S.O.: J. Korean Phys. Soc. **66**, 790 (2015)
28. Vijayaprasath, G., Murugan, R., Mahalingam, T., Hayakawa, Y., Ravi, G.: J.Alloys Compd. **649**, 275 (2015)
29. Ye, L.H., Freeman, A.J., Delley, B.: Phys. Rev. B. **73**, 033203 (2006)
30. Van, L.H., Ding, J., Hong, M.H., Fan, Z.C.: Surf. Rev. Lett. **15**, 81 (2008)
31. Mishra, D.K., Kumar, P., Sharma, M.K., Das, J., Singh, S.K., Roul, B.K., Varma, S., Chatterjee, R., Srinivasu, V.V., Kanjilal, D.: Physica B: Cond. Matter. **405**, 2659 (2010)
32. Ekicibil, A., Bulun, G., Çetin, S., Dikmen, Z.: J. Supercond. Nov. Magn. **25**, 435 (2012)
33. Cao, X., Meng, J., Mi, F., Zhang, Z., Sun, J.: Solid State Commun. **151**, 678 (2011)
34. Rubi, D., Fontcuberta, J., Calleja, A., Aragones, L.: Phys. Rev. B. **75**, 155322 (2007)

Publisher's note Springer Nature remains neutral with regard to jurisdictional claims in published maps and institutional affiliations.